

Nanoscale Advances

Accepted Manuscript

This article can be cited before page numbers have been issued, to do this please use: M. Oliel and Y. Mastai, *Nanoscale Adv.*, 2025, DOI: 10.1039/D4NA01006J.



This is an Accepted Manuscript, which has been through the Royal Society of Chemistry peer review process and has been accepted for publication.

Accepted Manuscripts are published online shortly after acceptance, before technical editing, formatting and proof reading. Using this free service, authors can make their results available to the community, in citable form, before we publish the edited article. We will replace this Accepted Manuscript with the edited and formatted Advance Article as soon as it is available.

You can find more information about Accepted Manuscripts in the [Information for Authors](#).

Please note that technical editing may introduce minor changes to the text and/or graphics, which may alter content. The journal's standard [Terms & Conditions](#) and the [Ethical guidelines](#) still apply. In no event shall the Royal Society of Chemistry be held responsible for any errors or omissions in this Accepted Manuscript or any consequences arising from the use of any information it contains.

DOI: 10.1039/x0xx00000x

Received 00th January 20xx,
Accepted 00th January 20xx

Chiral induction in the crystallization of KIO_3 and LiIO_3 , the role of amino acids in controlling the chirality of inorganic crystals.

Matan Oliel,^{*a} and Yitzhak Mastai^b

Department of Chemistry and Institute of Nanotechnology, Bar-Ilan University, Ramat-Gan 5290002, Israel

Chiral induction in crystals attract significant attention due to its implications for developing chiral materials and understanding mechanisms of symmetry-breaking enantioselective crystallization of naturally occurring chiral minerals. Despite its potential use in chiral discrimination, this area remains largely unexplored. Here, we investigate chiral induction during crystallization of naturally occurring chiral KIO_3 and LiIO_3 minerals using arginine and alanine as chiral inducers. The chiral nature of the crystallization and the effect of the chiral inducers were examined using circular dichroism, polarimetry, and low-frequency Raman spectroscopy. The impact of chiral molecules on the rate and final crystal structure was studied by electron microscopy including SEM and TEM. We demonstrate that it is possible to control the chirality with chiral exogenous molecules, mainly amino acids. Understanding chiral induction in crystal growth may open avenues for controlled assembly of chiral materials and development of novel functional materials with unique properties.

Introduction

Chirality is often associated with organic molecules; however, many inorganic compounds also exhibit chirality in their crystal structures. This chirality in inorganic crystals generally results from a chiral arrangement of non-centrosymmetric metal chelates or oxides. For instance, quartz (SiO_2) demonstrates chirality in its α polymorph due to the chiral arrangement of SiO_2 units.

Studying the chirality of chiral inorganic crystals is surprisingly limited¹. The surface of chiral inorganic crystals holds significant promise for various applications including chiral discrimination²⁻⁵, chiral sensing⁶ and enantioselective catalysis^{7,8}. Understanding how surface chirality is influenced

by chiral induction and controlling chirality in these materials is crucial, as chiral selectivity occurs primarily on the material surface⁹.

In recent years, chirality has been found to play an important role in nanotechnology¹⁰⁻¹². Chirality plays a useful role in many nano-systems, such as chiroptical molecular switches¹³⁻¹⁵, molecular motors, chiral nanosurfaces¹⁶⁻²⁶ and chiral nanoparticles²⁷⁻³⁹. Overall, the areas of chiral nanoscience and nanotechnology show exceptionally strong promise for further developments in areas such as catalysts, bio-recognition and chiral separation processes⁴⁰.

One good example of chiral surfaces is chiral selectivity on metal surfaces that are well-established, in particular with cubic closed-packed (CCP) metals⁴¹. Crystal planes such as Cu

^a Address here.^b Address here.^c Address here.

† Footnotes relating to the title and/or authors should appear here.

Supplementary Information available: [details of any supplementary information available should be included here]. See DOI: 10.1039/x0xx00000x



(6,4,3) and Au (3,2,1) exhibit chiral properties despite the lack of chirality of bulk metals. These surface features yield exceptional enantiomeric excess (e.e) during adsorption of small chiral molecules^{4,42}.

In recent decades, remarkable strides were taken in exploring the nature of inorganic chiral surfaces and systems. Pioneering research led by the Gellman group unveiled the chirality of high-Miller-index planes in metallic surfaces, revealing their enantiospecific adsorption in the presence of chiral molecular probes^{6,17}. Research led by Hazen and collaborators emphasized the significance of chiral inorganic crystal surfaces, in particular in mineral-catalyzed organic synthesis and the interactions between biomolecules and mineral surfaces^{1,43,44}. In a series of publications, Hazen *et al.* carefully documented numerous common rock-forming minerals, predominantly chiral oxides and silicates, which exhibit chiral crystal surfaces, showcasing the chiral selection of amino acids on these surfaces^{45,46}.

However, naturally occurring chiral minerals including quartz (SiO₂)⁴⁷, Monohydrocalcite (CaCO₃·H₂O)⁴⁸, Wulfingite (ε-Zn(OH)₂)⁴⁹ and α-HgS^{50,51} received little attention. Some chiral minerals are believed to contribute to the development of homochirality in biological molecules through an extensive process of chiral discrimination^{52,53}. Studying the influence of chiral amino acids on formation of chiral minerals and replicating the natural conditions in which this occurs provides valuable insights into these processes. This research can also elucidate mechanisms that control chiral biomolecules. While some chiral minerals form the chiral phase in a straightforward manner, the crystallization of certain chiral crystals is more complex. For example, Berlinite, the quartz-like chiral form of AlPO₄, requires high annealing temperatures to transform into its chiral phase^{54,55}. These extreme conditions present challenges for analysis of chiral induction.

To address this issue, we sought chiral inorganic systems that crystallize under relatively simple conditions, mainly at low temperature and in aqueous solutions. Potassium iodate (KIO₃)^{56,57} and lithium iodate (LiIO₃)^{58,59} are perfect examples. KIO₃ and LiIO₃ are naturally occurring chiral minerals with space groups of P1 and P6322, respectively, which are easy to crystallize, and their chiral phases are stable at room temperature (RT). As water-soluble salts, their chirality and chiral induction were apparently not investigated.

Here, we present our research on control of chirality of KIO₃ and the LiIO₃ crystals by chiral induction with amino acids. The crystal morphology and structural changes were confirmed by X-ray diffraction (XRD), Fourier transform infrared (FTIR) spectroscopy and high-resolution scanning electron microscopy (HR-SEM). Moreover, the chirality was

analyzed by circular dichroism (CD) spectroscopy of crystal pellets and optical polarizer for low-frequency Raman (LFR). The enantioselectivity and chiral discrimination was proved by CD and polarimeter by chiral adsorption experiments.

Experimental methods

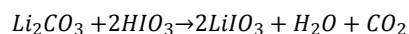
Materials

The materials used in this research are detailed in the supporting information (S1).

Preparation of chiral-induced crystals

Chiral-induced KIO₃ crystals were synthesized by recrystallization with slow cooling method. Supersaturated solutions in double distilled water (DDW) were prepared, heated to 50 °C and stirred until complete dissolve. After dissolution, 10% (moles / to KIO₃ moles) of L/D-Arg were added and the solution was stirred for 15 min and spontaneously cooled to RT by turning off the hot plate and keep the solution on it to allow as slow as possible cooling process and then the solution refrigerated overnight. The white crystals were filtered in vacuum, washed several times with ethanol to remove Arg traces and dried at RT.

The chiral-induced LiIO₃ crystals were synthesized by slow evaporation method using the following reaction:



In a typical case 0.5 g of lithium carbonate (Li₂CO₃) and 2.375 g of iodic acid (HIO₃) were dissolved in 20 mL of DDW. The solutions were put in oil bath and heated to 60 °C under stirring at pH = 10 to allow the reaction to occur. The basic conditions were achieved by adding lithium hydroxide (LiOH). After dissolution, 60.6 mg of L/D-Ala (10% mole of Li₂CO₃) were added and the solution was covered by pierced aluminum foil to prevent contamination and allow evaporation. The stirring was stopped after 24 h and the heating was kept at 60 °C in oil bath to maintain constant temperature until complete evaporation. To remove residual Ala, clear white crystals were soaked for 24 hours in 9:1 MeOH/DDW in a glass beaker. The cleaned crystals were filtered and dried in an oven at 50 °C.

Characterization methods

The crystallographic structures of KIO₃ and LiIO₃ were determined by XRD using a Bruker AXS D8 Advance diffractometer with Cu Ka (λ = 1.5418 Å) operating at 40 kV/40 mA, collecting from 10 to 80 °.

FTIR was performed using a Thermo Scientific Nicolet iS10 spectrometer equipped with a Smart iTR attenuated total reflectance sampler with a single bounce diamond crystal.



Data was collected in the 530–4000 cm^{-1} range at a spectral resolution of 4 cm^{-1} and analyzed using OMNIC software.

HR-SEM images were taken using a field-emission FEI (Helios 600) instrument. Samples were sputtered with gold.

KIO₃ and LiIO₃ crystal's chirality measurements

Pellets (KBr, 300 mg, 5/10% L/D-induced Li/KIO₃) were prepared (mixed and pressed under 10 ton for 3 min) and measured by CD in a designated holder at different orientations at RT with a Chirascan spectrometer (Applied Photophysics, UK).

LFR was carried out on a Via Raman microscope (Renishaw, UK) at RT under optical microscope with a 50 \times objective. The samples were excited using a 514 nm laser source with a P-polarization (vertical) ratio of 100:1 (0.5 mW, 40 s) and spectra were acquired using a polarizer with 1800 l/mm grating in the range of 100–1500 cm^{-1} .

Chiral adsorption onto KIO₃ and LiIO₃ crystals

Tartaric acid (TA) was chosen due its solubility in ethanol in which KIO₃ and LiIO₃ are insoluble. Chiral adsorption measurements were carried out with CD by preparing a 2.5 mM solution of D/L-TA or DL-TA in ethanol and adding L-Arg-induced KIO₃ crystals or L/D-Ala-induced LiIO₃ in several concentrations. The crystals were kept suspended in solution overnight using a rotary suspension mixer and filtered out using a 0.2 mm filter. The filtered solutions were taken to CD measurement and compared to pure D/L-TA or DL-TA solutions.

Chiral adsorption by polarimeter was performed by preparing a 5 wt% solution of D/L-TA in ethanol and adding L-Arg-induced KIO₃ or L-Ala-induced LiIO₃ crystals in several concentrations. The crystals were kept suspended in solution overnight using a rotary suspension mixer and filtered out using a 0.2 mm filter. The filtered solutions were taken to polarimeter measurement and compared to pure D/L-TA solutions. The solutions were measured at RT by a Jasco P-2000 polarimeter.

The selectivity was calculated by measuring the polarization ratio of the enantiomer (adsorption peak maxima) with respect to the pure enantiomer.

For the selectivity measurement by mass change were carried out by preparing a 20 mM of D/L-TA solution in ethanol and adding D-Ala-induced LiIO₃ in concentration of 32 mg/mL. The crystals were kept suspended in solution overnight using a rotary suspension mixer and filtered out using a 0.2 mm filter. The filtered solutions were evaporated and the mass change calculated compared to the mass of D/L-TA before the adsorption.

Results and discussion

Characterization

First, we studied the changes in structure and morphology by XRD and FTIR following chiral induction by amino acids. In all samples, the main crystalline structure of KIO₃ at RT was the stable triclinic phase with chiral space group P1 (COD ID: 4318187) and main diffraction peak at $2\theta = 28.2^\circ$ corresponding to its (2, -2, 2) plane (Figure 1I). The cell units a, b, c are 8.923, 8.942, 7.709 Å and α, β, γ are 54.4, 125.3, 90.6°. The unchanged diffractions indicate that the crystalline structure is maintained. LiIO₃ displays a crystalline structure that fits the RT stable hexagonal phase with chiral space group P6₃22 (COD ID: 1529711). The key diffraction peak at 25.5° corresponds to the (1, 0, 1) plane (Figure 1II). The unit cell dimensions were a = 5.478 Å, b = 5.478 Å, c = 5.17 Å with $\alpha = \beta = 90^\circ$ and $\gamma = 120^\circ$. Similar to KIO₃, the consistent results indicate that the structure was maintained.

We also characterized the crystals by FTIR to check for structural changes or traces of amino acid. Both pristine and chiral-induced KIO₃ showed the same spectra and indicated two peaks, close to each other, with a broad peak at 722 cm^{-1} and a very small peak at 797 cm^{-1} . Both peaks represent the vibration modes of the oxygen-iodine bonds (Figure S2I). Similarly, the LiIO₃ crystals showed two peaks belonging to the O-I vibration modes and no difference between the pristine and chiral induced crystals (Figure S2II). However, we noticed a redshift at 763 and 860 cm^{-1} probably due to the effect of the cation on the vibration mode energies in the lattice. Moreover, the control LiIO₃ sample also has a broad absorbance peak between 1400, and 1700 cm^{-1} associated with C=O indicating some unreacted Li₂CO₃.



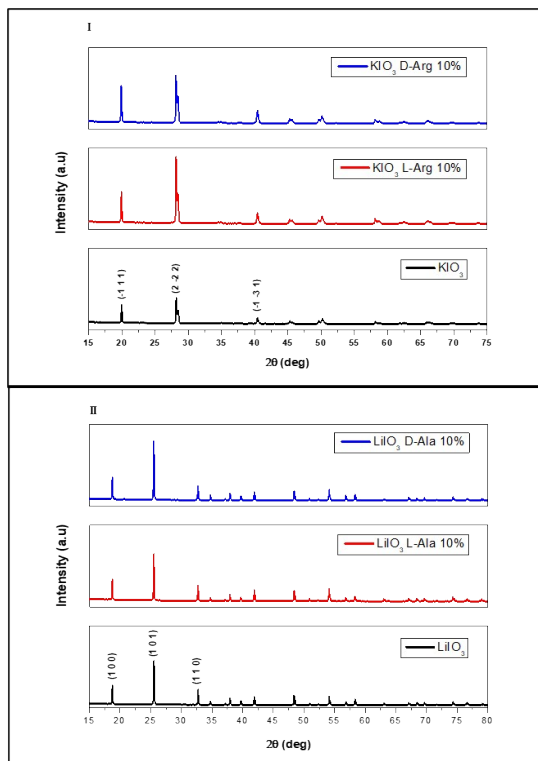


Figure 1 – XRD of KIO_3 (I) and LiIO_3 crystals (II) – control (black), L-Arg-induced (red) and D-Arg-induced (blue) displaying the main diffraction planes of triclinic KIO_3 and hexagonal LiIO_3 .

Morphology and surface analysis

The morphology was examined by HR-SEM. The control KIO_3 crystals exhibit a square shape and smooth surface (Figure 2I, IV) however, with the amino acid the morphology and surface change. The L-Arg-induced KIO_3 crystals maintain a square shape albeit with a rough surface (Fig. 2II, V), while the D-Arg-induced KIO_3 crystals are hexagonal with a smooth surface similar to the control (III, VI).

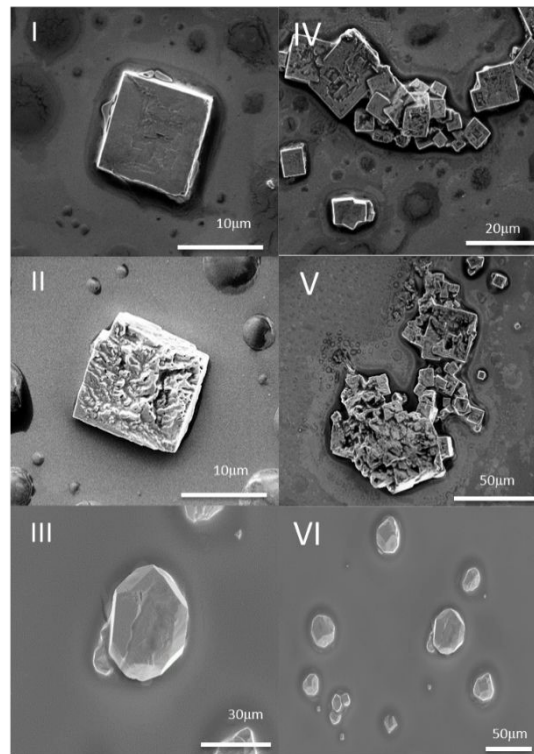


Figure 2 – HR-SEM images of KIO_3 crystals – control (I, IV / 10, 20 μm), L-Arg-induced KIO_3 (II, V / 10, 50 μm) and D-Arg-induced KIO_3 (III, VI / 30, 50 μm).

Figure 3 presents HR-SEM images of LiIO_3 crystals. Pristine LiIO_3 shows an uneven morphology and very rough surface (I, IV). In contrast, L-Ala-induced LiIO_3 crystals have a more hexagonal shape with a smoother surface (II, V). D-Ala-induced LiIO_3 crystals have an uneven morphology similar to pristine LiIO_3 with a rougher surface, which is smoother than the surface of pristine LiIO_3 (III, VI).

Nanoscale Advances Accepted Manuscript



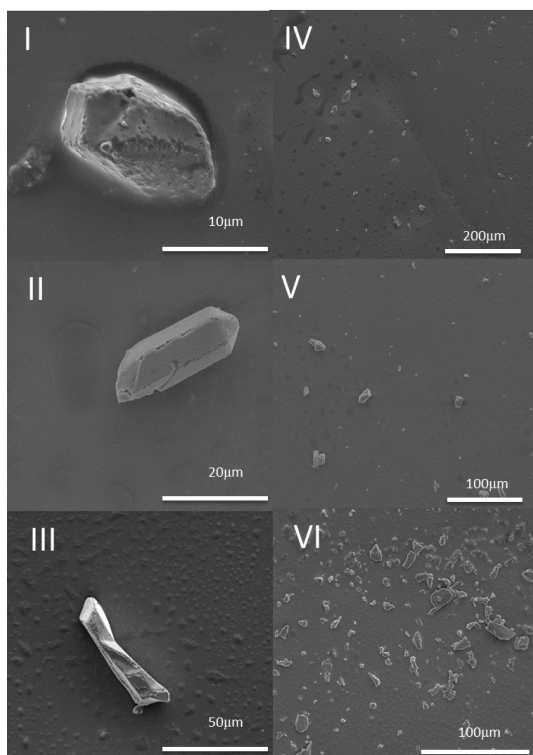


Figure 3 – HR-SEM images of LiIO_3 crystals – control (I, IV / 10, 200 μm), L-Ala-induced LiIO_3 (II, V / 20, 100 μm) and D-Ala-induced LiIO_3 (III, VI / 50, 100 μm).

Direct chirality measurements

To prove the chiral preference, we measured the crystals with CD and LFR. For CD measurement, L/D-Arg-induced KIO_3 and L/D-Ala-induced LiIO_3 pellets were prepared and measured at different angles. The CD measurement of the chiral-induced KIO_3 crystals show two chiral signal areas: a wide one from 525 to 275 nm, and narrow one below 525 nm.

Moreover, a positive signal is seen for the D-Arg-induced crystals and a negative one (anticlockwise direction polarization) for L-Arg-induced KIO_3 (Figure 4I). In contrast, LiIO_3 (Figure 4II) presents opposite signals – positive for L-Ala-induced LiIO_3 and negative for D-Ala-induced LiIO_3 . LiIO_3 crystals also display a wide chiral signal from 600 to 400 nm. Both CD spectra show the optical activity of the iodate crystals proving their chiral preference.

While this measure does not provide absolute chirality, the relative purity can be obtained by the most frequent polarizations. The polarization of L-Ala-induced LiIO_3 is +4 mdeg vs. -6 mdeg for D-Ala-induced LiIO_3 , thus the latter crystals are 1.5 times purer. L-Arg-induced KIO_3 is 1.2 times purer than the D-Arg-induced crystals (-15/+12.5 mdeg for L/D-Arg-induced KIO_3).

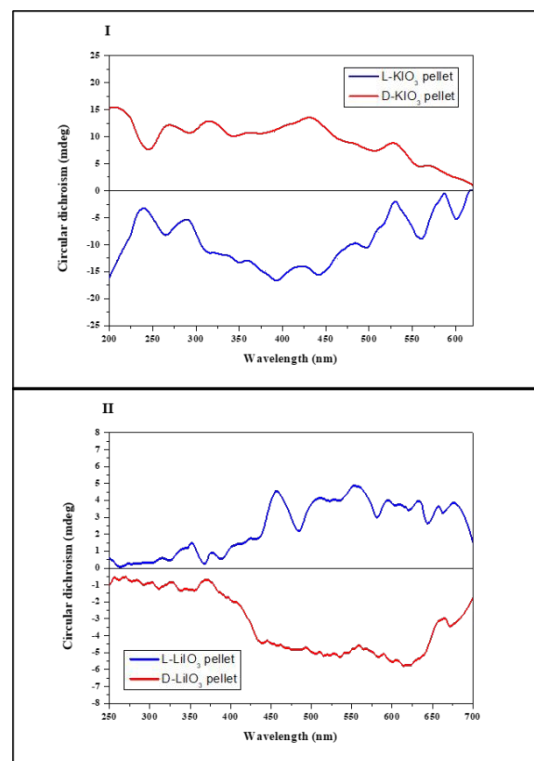


Figure 4 – CD spectra of L/D-Arg-induced KIO_3 (I) and L/D-Ala-induced LiIO_3 (II) pellets.

The chirality was also measured by low frequency Raman spectroscopy (LFR)⁶⁰, a new technique that allows direct measurement of the chirality employing the low-frequency region of the spectrum, which highlights lattice-level interactions and global molecular fluctuations. These lower frequencies are associated with vibrations from weaker bonds and long-range interactions making them highly sensitive to changes in polarization. The enantiomers are excited by fixed polarized light and collected using a movable optical polarization. The polarized light can be horizontal (S-Pol) or vertical (P-Sol). One enantiomer gives a stronger signal for S-Pol, while the other gives a stronger signal for P-Pol.

Aviv *et al.* presented a method that differentiates racemic and enantiopure crystals of amino acids. Intensity changes and wavenumber shifts were seen in single crystals of arginine, aspartic acid and valine⁶¹. Nematsov *et al.* used LFR to analyze the chiral purity of crystals and showed specific vibrational mode changes as a function of the enantiomeric purity⁶². Moreover, they investigated the dependence of the signal intensity on the orientation of L-Ala single crystals showing correlation between signal intensities with the proximity between the incident beam direction and the orientations of the intermolecular interactions⁶³. This makes LFR a powerful method to prove chiral preference by direct measurement.



As iodate salts, the Raman spectroscopy of KIO_3 and LiIO_3 are quite similar (Figure S3) and can be divided to three areas: $700\text{--}800\text{ cm}^{-1}$ (iodate vibrational modes), $300\text{--}400\text{ cm}^{-1}$ (free translational motion of the iodate anion) and $100\text{--}200\text{ cm}^{-1}$ (lattice vibrational modes).

We used LFR method to examine the effect of KIO_3 and LiIO_3 chiral-induced crystals on the collection of light through a polarizer at different angles (S-Pol and P-Pol), where the enantiomers of the crystal under test are supposed to give opposite effects to each other in intensities at same angles. Moreover, in order to prove the effect precisely, the comparison is of the angles for each crystal separately when the light is collected from the same point in the sample in order to neutralize as many factors as possible that could affect the measurements.

Figure 5I presents the LFR of chiral induced crystals. Higher intensity is evident for the L-chiral inducing KIO_3 crystals when the light is collected at P-Pol with maximum intensity ratio P-Pol/S-Pol of 1.225 at 303 cm^{-1} . In contrast, D-Ala-induced LiIO_3 crystals produce higher intensity when the light is collected at S-Pol with maximum S-Pol/P-Pol intensity ratio at 329 cm^{-1} of 1.247 (Figure 5II).

The LFR results support previous measurements. Iodate crystals with higher P-Pol intensity are more prone to be L type, while those with higher S-Pol intensity tend to be D type crystals. Similar results were obtained for D-Arg-induced KIO_3 and L-Ala-induced LiIO_3 (Figure S4). LFR signifies long-range interactions where orientation-dependent polarizable interactions prevail. Such interactions are highly responsive to the symmetry of the excitation cone induced by the polarizer and thus provide insight into the crystal chirality.

After proving the chiral preference of our crystals, we used chiral adsorption methods to check their stereoselectivity and chiral discrimination.

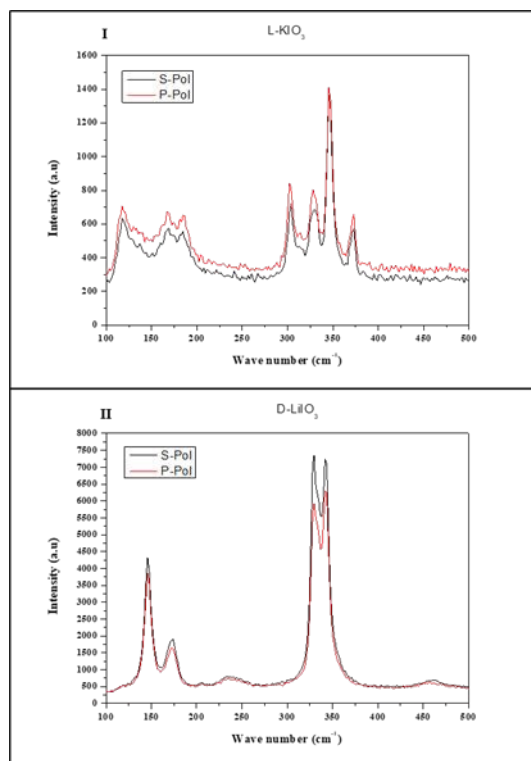


Figure 5 - LFR spectra of L-Arg-induced KIO_3 (I) and D-Ala-induced LiIO_3 (II). Black/red curves show signals excited using S/P-Pol.

Chiral selectivity measurements

The adsorption of chiral molecules onto chiral surfaces is a standard way of measuring chirality in solids. Here, we measured the chiral induction on L-Arg-induced KIO_3 and L/D-Ala-induced LiIO_3 using CD and polarimeter. In the CD adsorption experiment, a 2.5 mM solution of pure L/D-TA was adsorbed at RT onto different powder concentrations. Figure 6I presents the CD adsorption at 32 mg/mL. The control group which contains the KIO_3 without chiral inducer showed adsorption of $\sim 5\%$ for both L and D-TA without any selectivity at all (green and cyan curves, respectively). However, the addition of the L-Arg to the KIO_3 crystals led to adsorption of 7% for L-TA (red curve) compared to pure L-TA (black curve) and better adsorption of (18%) onto D-TA (pink curve) compared to pure D-TA (blue curve). Figure 6II shows the selectivity of both enantiomers to L-Arg-induced KIO_3 ; we see better selectivity at all concentrations to D-TA (up to 11%). Moreover, the difference between the enantiomers



increases with increasing concentrations of L-Arg-induced KIO_3 crystals.

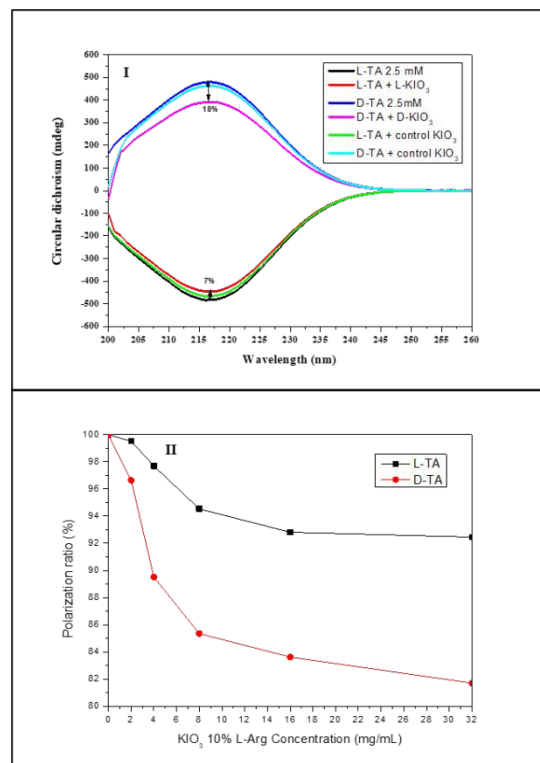


Figure 6 – Selective chiral adsorption of TA on chiral L-Arg-induced KIO_3 crystals: CD spectra of L/D-TA adsorbed onto L-Arg-induced KIO_3 (I) and selectivity of L/D-TA at different concentrations (II).

Figure 7I illustrates the CD adsorption at a concentration of 32 mg/mL. Like KIO_3 , the control group of un-inducing LiIO_3 doesn't displayed discernible selectivity with an adsorption of about 20% for both L and D-TA (orange and purple curves, respectively). L-Ala-induced LiIO_3 demonstrates enhanced adsorption for L-TA (48%, red curve) compared to pure L-TA (black), while D-TA exhibits 38% absorption (cyan). Superior selectivity is seen at all concentrations, which increases with the crystal concentration up to 10% (Figure 7III). D-Ala-induced LiIO_3 on the other hand shows better adsorption for D-TA (34%, green curve) compared to pure D-TA (pink), while L-TA exhibits 23% absorption onto D-Ala-induced LiIO_3 (blue). D-Ala-induced LiIO_3 crystals show better selectivity for D-TA at all concentrations, with quite similar values up to 11% (Figure 7II).

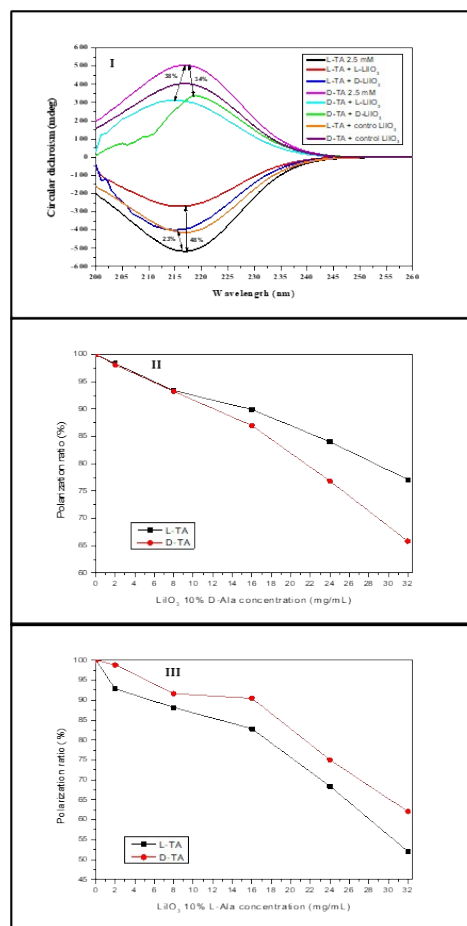


Figure 7 – Selective chiral adsorption of TA on chiral induced LiIO_3 crystals – CD spectra of L/D-TA adsorbed onto L/D-Ala-induced LiIO_3 (I) and selectivity at different D/L-Ala-induced LiIO_3 concentrations (II/III).

To verify that the results obtained indeed show selectivity of the crystals, two additional measurements were made: measuring the mass change of TA enantiomer that did not adsorb onto the crystals after evaporation of the solvent, and measuring the circular dichroism of racemic solution of TA in order to identify any chiral sign which point to selectivity of the crystals.

Table 1 shows the results for the mass changes of the TA enantiomer that did not adsorb onto the D-Ala-induced LiIO_3 crystals after filtration of the crystals and evaporation of the solvent. We can see that the D-TA mass decreased more (25%) than the L-TA mass (15%) which means the D-Ala-induced LiIO_3 crystals are selective in favor to D-TA. Moreover, we notice that the selective percentages are similar to the selectivity we received from the CD (11% and 10% respectively).



Crystal	D-Ala-LiIO ₃	
	L-TA	D-TA
Tested enantiomer	L-TA	D-TA
Vial mass (mg)	17683.5	17753.1
Total mass (mg)	17693.7	17762.1
Unadsorbed TA mass (mg)	10.2	9
Decrease from total mass (%)	15	25
Selectivity (%)	10 in favor of D-TA	

Table 1 - Selective chiral adsorption of TA onto D-Ala-induced LiIO₃ crystals by measuring the TA mass changes after crystals filtration and solvent evaporation.

Figure 8 presents the circular dichroism measurement of the racemic solution of TA that did not adsorb onto the D-Ala-induced LiIO₃ crystals. The measurement shows negative signals of the solution that indicate a higher presence for the L-TA enantiomer which means the D-Ala-induced LiIO₃ crystals are chiral selective in favor to D-TA.

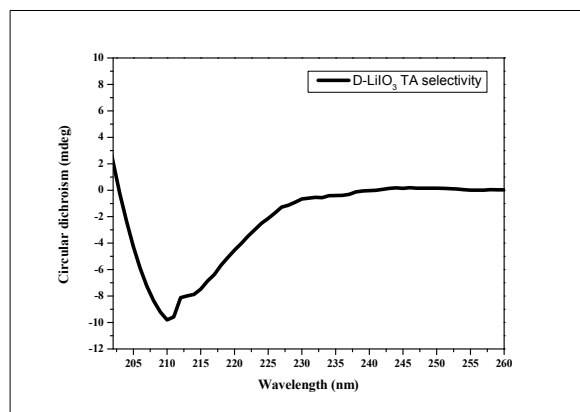


Figure 8 – Selective chiral adsorption of DL-TA on D-Ala-induced LiIO₃ crystals.

We also examined the selective chiral adsorption on the crystal surfaces by polarimeter. The polarimeter adsorption experiment included pure L/D-TA 5wt% solution that adsorbed onto L-Arg-induced KIO₃ crystals powder concentrations (2, 4, and 8 mg/mL) at RT. Figure 9 presents the selectivity of both TA enantiomers to the L-Arg-induced KIO₃ crystals, and like the CD measurements, we can see better selectivity for the D-TA enantiomer for all concentrations. The L-Arg-induced KIO₃ shows maximum adsorption of 7% for L-TA at the most concentrated KIO₃ compared to the D-TA at the same crystal concentration with maximum adsorption of 24%, therefore, the maximum selectivity we got was 17%. Moreover, we saw by polarimeter the selectivity improvement proves as function of L-Arg-induced KIO₃ crystals concentration increase. From the results obtained it can be noted that there is a difference of 6% between the maximum selectivity of L-Arg-induced KIO₃ we got from the CD measurements and from the polarimeter. The difference can be explained by the lower sensitivity of the polarimeter which required more concentrated solutions for

measurements that affect the amount of the TA adsorbed onto the L-Arg-induced KIO₃.

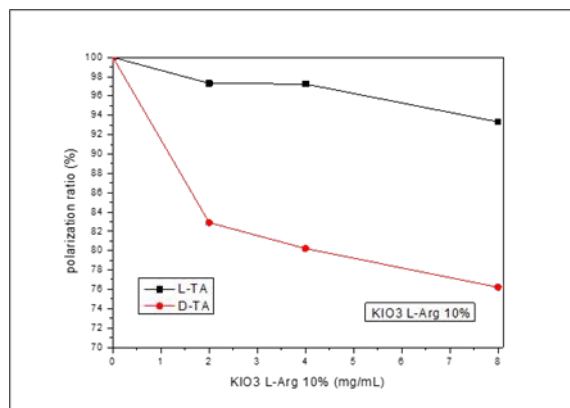


Figure 9 - Chiral selective adsorption of TA on L-Arg-induced KIO₃ crystals by polarimeter.

Chiral separation by crystallization⁶⁴⁻⁶⁷ is a well-established method whereby a chiral substance such as a chiral resolving agent or solvent is introduced in the crystallization of a racemic mixture. This method typically involves the chiral agent interacting differently with the crystals of each enantiomer during crystallization. In our case, the chiral separation is likely due to the interaction of amino acids with ionic crystal surfaces in a chiral-specific manner. This interaction can influence the nucleation and growth processes by preferentially stabilizing one enantiomer over another. A kinetic study assessed the impact of amino acids on crystallization and chiral separation. Figure 9 shows results for samples collected at various stages of crystallization.

The normal crystallization of KIO₃ shows after 4 h crystals with uniform rhombus shape and relatively uniform size of 4.5 μm (Figure 10I). After 12 h crystals of various sizes were obtained resembling a dodecahedron structure with 25 μm size (Figure 10IV). The chiral induced crystallization presents a different phenomenon: L-Arg-induced KIO₃ shows an arrangement of square crystals on top of each other that resembles terraces (Figure 10II, V), while D-Arg-induced KIO₃ shows such arrangement after 12 h (Figure 10VI) and a trapezoid structure with average size of 4 μm after 4 h (Figure 10III).

It should be noted that we investigated the effect of amino acid concentration on both the crystallization process and chiral induction in the crystals. A series of crystallization experiments were conducted at varying amino acid concentrations, ranging from 1% to 10% by weight relative to the crystal-forming ions. It was found that at concentrations below 10%, no chiral induction was observed. However, starting at 10% (w/w) and above, chiral induction effects were detected and maintained. At higher amino acid



concentrations, no further enhancement in chiral induction was observed.

Our results suggest that amino acids can promote the formation of mesocrystals^{68,69} by facilitating the organization of nanocrystals into ordered aggregates. Mesocrystals are crystalline materials consisting of nanometer-sized building blocks often referred to as "nanocrystals" arranged in a regular, repeating pattern. Unlike traditional crystals, composed of a continuous lattice of atoms or molecules, mesocrystals are made up of these smaller, ordered nanocrystals that can be connected in various ways. Overall, it appears that during nucleation amino acids preferentially bind to one chiral face of the crystal, influencing the nucleation rate, resulting in the observed chiral separation.

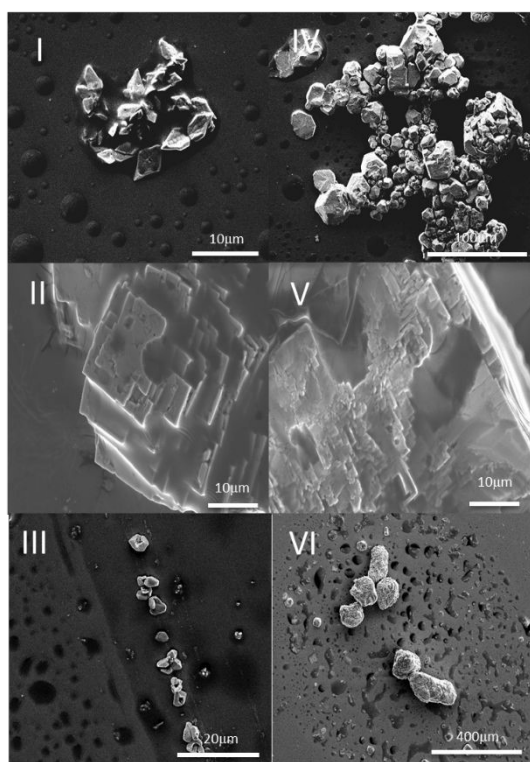


Figure 10 - HR-SEM images of kinetic crystallization of KIO_3 – control KIO_3 crystals after 4/12 h (I/IV, 10/100 μm), L-Arg-induced KIO_3 after 4/12 h (II/V, 10/10 μm) and D-Arg-induced KIO_3 after 4/12 h (III/VI, 20/400 μm).

Conclusions

Chiral induction of the naturally occurring chiral iodate salt minerals KIO_3 and LiIO_3 was achieved using chiral alanine and arginine. The resultant crystals varied in morphology, size and surface roughness in contrast to the uniform crystallization obtained without chiral induction. The most prominent change was in the KIO_3 crystals, which transformed from

square to hexagonal/deformed shape in D/L-Arg-induced KIO_3 . Both chiral-induced LiIO_3 crystals exhibited smoother surfaces. L-Ala-induced LiIO_3 retained a hexagonal shape, whereas D-Ala-induced LiIO_3 displayed an uneven morphology.

The effect of the chiral induction on KIO_3 kinetics was investigated by crystallization at different times. The presence of the chiral inducing molecules was found to affect the arrangement of the KIO_3 crystals by creating mesocrystals with terrace arrangement.

The chiral preference of our crystals was confirmed by various direct measurements including CD of crystal pellets and LFR powder spectroscopy. Significantly, both methods were found to be applicable for direct measurement of the crystal chirality.

The enantioselectivity was also assessed by chiral adsorption measurements on the crystal surface using CD spectroscopy and polarimetry. While L-Arg-induced KIO_3 crystals showed higher selectivity for D-TA, L-Ala-induced LiIO_3 showed higher selectivity for L-TA. These findings indicate that L/D-induced crystals do not necessarily improve selectivity for L/D-enantiomers; better improvement may be obtained for the other enantiomers. It should be noted that while our study primarily focuses on chiral induction, we recognize that the reversibility of this process is a crucial factor in understanding the underlying mechanisms. Many chiral crystallization studies have shown that chiral induction by chiral molecules can, in some cases, be reversible under specific conditions, such as changes in pH, temperature, or solvent environment. However, in our experiments, once chirality was induced in the crystallized products, no spontaneous reversal was observed under the experimental conditions used.

Overall, this study provides insight on the chirality of iodate salt crystals within their chiral space group. Study of the chirality and chiral discrimination of naturally occurring chiral minerals such as KIO_3 and LiIO_3 is important for understanding the origin of biochemical homochirality and life. Integration of chiral amino acids in the crystallization of naturally occurring chiral minerals is anticipated to provide deeper insight and a more nuanced understanding of the intricate interactions between chiral molecules and crystal surfaces. This approach holds promise for elucidating mechanisms underlying chiral discrimination in inorganic crystals as a holistic process. Utilizing chiral recognition on inorganic surfaces offers advantages across various applications, from asymmetric autocatalysis to chiral sensing and optical functionalities.



AUTHOR INFORMATION

Department of Chemistry and Institute for Nanotechnology and Advanced Materials, Bar-Ilan University, Ramat Gan 5290002.

Corresponding Author

Prof. Yitzhak Mastai - Yitzhak.Mastai@biu.ac.il

Authors

Matan Oliel - matanoliel5@gmail.com

Notes

The authors declare no competing financial interest.

Conflicts of interest

There are no conflicts to declare.

ASSOCIATED CONTENT

Supporting information is available free of charge via the Internet at: <http://pubs.acs.org>.

Materials, and FTIR spectra of L/D-Arg-induced KIO₃ and L/D-Ala-induced LiIO₃ crystal (PDF).

ACKNOWLEDGMENT

MO acknowledges the Institute for Nanotechnology and Advanced Materials at Bar-Ilan University for his Bar-Ilan President's Ph.D. Scholarship.

Notes and references

- 1 D. Aquilano, F. Otálora, L. Pastero, and J.M. García-Ruiz, *Progress in Crystal Growth and Characterization of Materials*, 2016, **62** (2), 227-251.
- 2 W. Xu, M. Cheng, S. Zhang, Q. Wu, Z. Liu, M.K. Dhinakaran, F. Liang, E.G. Kovaleva, and H. Li, *Chemical Communications*, 2021, **57** (61), 7480-7492.
- 3 N. Nandi, and D. Vollhardt, *Current Opinion in Colloid & Interface Science* 2008, **13** (1-2), 40-46.
- 4 D.S. Sholl, A. Asthagiri, and T.D. Power, *The Journal of Physical Chemistry B*, 2001, **105** (21), 4771-4782.
- 5 J.I. Putman and D.W. Armstrong, *Chirality*, 2022, **34** (10), 1338-1354.
- 6 J.D. Horvath and A.J. Gellman, *Journal of the American Chemical Society*, 2002, **124** (10), 2384-2392.
- 7 C.E. Song, and S.G. Lee, *Chemical Reviews*, 2002, **102** (10), 3495-3524.
- 8 A. Matsumoto, Y. Kaimori, M. Uchida, H. Omori, T. Kawasaki, and K. Soai, *Angewandte Chemie International Edition*, 2017, **56** (2), 545-548.

- 9 T. Cao, Y. Li, L. Tian, H. Liang and K. Qin, *ACS Appl. Nano Mater*, 2018, **1** (2), 759-767.
- 10 D.B. Amabilino, *Chemical Society Reviews*, 2009, **38**, 669-670.
- 11 D.S. Bag, T.C. Shami and K.U.B. Rao, *Science Journal*, 2008, **58**, 626-635.
- 12 J. Zhang, M.T. Albelda, Y. Liu and J.W. Canary, *Chirality*, 2005, **17**, 404-418.
- 13 B.L. Feringa, N.P.M. Huck and A.M. Schoevaars, *Advanced Materials*, 1996, **8**, 681-&.
- 14 B.L. Feringa, R.A. van Delden, N. Koumura and E.M. Geertsema, *Chemical Reviews*, 2000, **100**, 1789-1816.
- 15 B.L. Feringa, *Accounts of Chemical Research*, 2001, **34**, 504-513.
- 16 X.Y. Zhao, S.S. Perry, J.D. Horvath and A.J. Gellman, *Surf Sci*, 2004, **563**, 217-224.
- 17 C.F. McFadden, P.S. Cremer and A.J. Gellman, *Langmuir*, 1996, **12**, 2483-2487.
- 18 K.H. Ernst, *Current Opinion in Colloid & Interface Science*, 2008, **13**, 54-59.
- 19 A.J. Gellman, *ACS Nano*, 2010, **4**, 5-10.
- 20 A. Kuhnle, T.R. Linderoth and F. Besenbacher, *Top Catal*, 2011, **54**, 1384-1391.
- 21 S.M. Barlow and R. Raval, *Surface Science Reports*, 2003, **50**, 201-341.
- 22 Y. Mastai, *Chemical Society Reviews*, 2009, **38**, 772-780.
- 23 L. Thomsen, A. Tadich, D.P. Riley, B.C.C. Cowie and M.J. Gladys, *Journal of Physical Chemistry C*, 2012, **116**, 9472-9480.
- 24 R. Oda, F. Artzner, M. Laguerre and I. Huc, *Journal of the American Chemical Society*, 2008, **130**, 14705-14712.
- 25 A.E. Baber, A.J. Gellman, D.S. Sholl and E.C.H. Sykes, *Journal of Physical Chemistry C*, 2008, **112**, 11086-11089.
- 26 C. Roth and K.H. Ernst, *Top Catal*, 2011, **54**, 1378-1383.
- 27 G. Shemer, O. Krichevski, G. Markovich, T. Molotsky, I. Lubitz and A.B. Kotlyar, *Journal of the American Chemical Society*, 2006, **128**, 11006-11007.
- 28 C. Gautier and T. Burgi, *Journal of the American Chemical Society*, 2006, **128**, 11079-11087.
- 29 C. Gautier and T. Burgi, *Journal of the American Chemical Society*, 2008, **130**, 7077-7084.
- 30 O. Álvarez-Bermúdez, K. Landfester, K.A.I. Zhang and R. Muñoz-Espí, *Macromolecular rapid communications*.
- 31 L.C. Preiss, M. Wagner, Y. Mastai, K. Landfester and R. Muñoz-Espí, *Macromolecular rapid communications*, 2016, **37**, 1421-1426.
- 32 L.C. Preiss, L. Werber, V. Fischer, S. Hanif, K. Landfester, Y. Mastai and R. Muñoz-Espí, *Adv. Mater*, **27**, 2728-2732.
- 33 P. Paik, Y. Mastai, I. Kityk, P. Rakus and A. Gedanken, *Journal of solid state chemistry*, 2012, **192**, 127-131.
- 34 R. Oda, I. Hue, M.C.D.J. Schmutz, S.J. Candau and F.C. MacKintosh, *Nature*, 1999, **399**, 566-569.
- 35 K. Sugiyasu, S.I. Tamaru, M. Takeuchi, D. Berthier, I. Hue, R. Oda and S. Shinkai, *Chemical communications*, 2002, **11**, 1212-1213.
- 36 F. Freire, J.M. Seco, E. Quiñoá and R. Riguera, *Angewandte Chemie International Edition*, 2011, **50**, 11692-11696.



- 37 F. Freire, J.M. Seco, E. Quiñoá and R. Riguera, *Journal of the American Chemical Society*, 2012, **134**, 19374-19383.
- 38 M. Lui, L. Zhang and T. Wang, *Chemical reviews*, 2015, **115**, 7304-7397.
- 39 L. Zhang, T. Wang, Z. Shen and M. Liu, *Advanced Materials*, 2016, **28**, 1044-1059.
- 40 T. Cao, L. Mao, Y. Qiu, L. Lu, A. Banas, K. Banas, R.E. Simpson and H.C. Chui, *ADVANCED OPTICAL MATERIALS*, 2019, **7 (3)**, 1801172.
- 41 J. Morales-Vidal, N.R. López, and M.A. Ortuño, *The Journal of Physical Chemistry C*, 2019, **123 (22)**, 13758-13764.
- 42 Ž. Šljivančanin, K.V. Gothelf, and B. Hammer, *Journal of the American Chemical Society*, 2002, **124 (49)**, 14789-14794.
- 43 A. Ben-Moshe, S.G. Wolf, M.B. Sadan, L. Houben, Z. Fan, A.O. Govorov, and G. Markovich, *Nature Communications*, 2014, **5 (1)**, 1-9.
- 44 R.M. Hazen, and D.A. Sverjensky, *Cold Spring Harbor Perspectives in Biology*, 2010, **2 (5)**, a002162.
- 45 W. Jiang, M.S. Pacella, D. Athanasiadou, V. Nelea, H. Vali, R.M. Hazen, J.J. Gray, and M.D. McKee, *Nature Communications*, 2017, **8 (1)**, 1-13.
- 46 R.M. Hazen, and D.S. Sholl, *Nature Materials*, 2003, **2 (6)**, 367-374.
- 47 Y. Tanaka, T. Takeuchi, S.W. Lovesey, K.S. Knight, A. Chainani, Y. Takata, M. Oura, Y. Senba, H. Ohashi, and S. Shin, *Physical Review Letters*, 2008, **100 (14)**, 145502.
- 48 G. Otis, M. Nassir, M. Zutta, A. Saady, S. Ruthstein, and Y. Mastai, *Angewandte Chemie*, 2020, **132 (47)**, 21110-21115.
- 49 P. Cintas, P, *Angewandte Chemie International Edition*, 2002, **41 (7)**, 1139-1145.
- 50 A. Ben-Moshe, S.G. Wolf, M.B. Sadan, L. Houben, Z. Fan, A.O. Govorov, and G. Markovich, *Nature Communications*, 2014, **5 (1)**, 1-9.
- 51 R.M. Hazen, T.R. Filley, and G.A. Goodfriend, *Proceedings of the National Academy of Sciences*, 2001, **98 (10)**, 5487-5490.
- 52 J. Jumas, A. Goiffon, B. Capelle, A. Zarka, J. Doukhan, J. Schwartzel, J. Detaint, and E. Philippot, *Journal of crystal growth*, 1987, **80 (1)**, 133-148.
- 53 Y. Muraoka, and K. Kihara, *Physics and Chemistry of Minerals*, 1997, **24 (4)**, 243-253.
- 54 P. Prado-Herrero, J. Garcia-Guinea, E. Crespo-Feo, and V. Correcher, *Phase Transitions*, 2010, **83 (6)**, 440-449.
- 55 L. Bayarjargal, L. Wiehl, and A. Friedrich et al, *J Phys Condens Matter*, 2012, **24 (32)**.
- 56 H. Kasatani, S. Aoyagi, Y. Kuroiwa, K. Yagi, R. Katayama, and H. Terauchi, *Nucl Instruments Methods Phys Res Sect B Beam Interact with Mater Atoms*, 2003, **199**, 49-53.
- 57 L. Liu, R.Q. Wu, Z.H. Ni, Z.X. Shen, and Y.P. Feng, *J Phys Conf Ser*, 2006, **28(1)**, 105-109.
- 58 R. Ashok Kumar, R. Ezhil Vizhi, N. Vijayan, and D. Rajan Babu, *Sch Res Libr*, 2011, **2(4)**, 373-383.
- 59 A. Silambarasan, P. Rajesh, and P. Ramasamy et al, *Bull Mater Sci*, 2017, **40(4)**, 783-789.
- 60 V. Damle, H. Aviv, and Y.R. Tischler, *Anal. Chem*, 2022, **94**, 3188-3193.
- 61 H. Aviv, I. Nematsov, Y. Mastai, and Y.R. Tischler, *J. Phys. Chem. A*, 2017, **121(41)**, 7882-7888.
- 62 I. Nematsov, Y. Mastai, Y.R. Tischler, and H. Aviv, *Chem. Phys. Chem*, 2018, **19(22)**, 3116-3121.
- 63 I. Nematsov, H. Aviv, Y. Mastai, and Y.R. Tischler, *Crystals*, 2019, **9(8)**, 425.
- 64 I. Weissbuch, L. Addadi, M. Lahav, and L. Leiserowitz, *Science*, 1991, **253(5020)**, 637-645.
- 65 G. Coquerel, *Novel Optical Resolution Technologies*, 2007, **269**, 1-51.
- 66 H. Lorenz, and A. Seidel-Morgenstern, *Angewandte Chemie*, 2014, **53(5)**, 1218-1250.
- 67 H. Cölfen, and M. Antonietti, *Angewandte Chemie*, 2005, **44(35)**, 5576-5591.
- 68 M. Niederberger, and H. Coelfen, *Physical Chemistry Chemical Physics*, 2006, **8(28)**, 3271-3287.
- 69 X. Xia, J. Tu, Y. Zhang, X. Wang, C. Gu, X. Zhao, H.J. Fan, *Acs Nano*, 2012, **6(6)**, 5531-5538.



View Article Online
DOI: 10.1039/D4NA01006J

ARTICLE

Open Access Article. Published on 05 mars 2025. Downloaded on 10/3/2025 15:01:27.
This article is licensed under a Creative Commons Attribution-NonCommercial 3.0 Unported Licence.



Nanoscale Advances Accepted Manuscript

Thursday, 21 November 2024

To

Prof. Dirk Guldi

Associate Editor, Nanoscale

Manuscript ID: NR-ART-09-2024-003843

Data Availability Statement

The data that support the findings of this study are available from the corresponding author upon reasonable request. Experimental data, including raw spectra and additional supplementary information, are included in the manuscript and its supporting files. Data not included in the manuscript are available upon request, and all relevant materials will be made accessible to qualified researchers for non-commercial purposes.

Sincerely,

Prof. Dr. Yitzhak Mastai



Tel: 03-531-7681 טל • Fax: 03-738-4053 פקס: E-mail: Mastai@biu.ac.il

אוניברסיטת בר אילן רמת גן 5290002, Israel 5290002 Bar-Ilan University Ramat Gan

www.biu.ac.il     

